Biosensors and Bioelectronics 146 (2019) 111744

Contents lists available at ScienceDirect

Biosensors and Bioelectronics

journal homepage: http://www.elsevier.com/locate/bios

Ultrasensitive biosensor for microRNA-155 using synergistically catalytic nanoprobe coupled with improved cascade strand displacement reaction

Zhixian Liang [a], Dan Ou [a], Duanping Sun [a,b], Yanli Tong [c,**], Haibin Luo [a,***], Zuanguang Chen [a,*]

[a] School of Pharmaceutical Science, Sun Yat-sen University, Guangzhou, 510006, China
[b] Center for Drug Research and Development, Guangdong Pharmaceutical University, Guangzhou, 510006, China
[c] Guangdong Second Provincial General Hospital, Guangzhou, 510317, China

ARTICLE INFO

Keywords:
microRNAs
Cu-NMOF
PtNPs
Co-catalytic nanoprobe
Improved toehold strand displacement reaction

ABSTRACT

MicroRNAs, essential for gene expression and physiological regulation, are considered to be reliable biomarkers for the early diagnosis and treatment of cancers. Herein, a sensitive biosensor that uses a synergistically catalytic nanoprobe and improved toehold strand displacement reaction (TSDR) has been fabricated, and successfully applied to microRNA-155 (miR-155) detection. A nanoscale copper-based metal organic framework assembled by Pt nanoparticles and horseradish peroxidase (Cu-NMOF@PtNPs/HRP) served as a co-catalytic nanoprobe and was coupled with improved TSDR to achieve multiple amplifications. In the absence of miR-155, the tetrahedral DNA nanostructures (TDNs) immobilized on the gold electrode were independent of the TSDR system because of the binding of the shielding region of the locked probe (LP) with the template probe (TP). Instead, the target would initiate the TSDR system, leading to the conformational change of TDNs and hybridization of the nanoprobe. Cu-NMOF@PtNPs/HRP exhibited extraordinary catalytic property towards the hydroquinone-hydrogen peroxide system, demonstrating that the nanoprobe exerted a concerted effect on the electrochemical performance of the biosensor. Under optimal conditions, the cathodic current exhibited a logarithmic relation over 0.50–1.0 × 10^5fM miR-155, with a detection limit of 0.13 fM, indicating that the constructed biosensor has considerable potential in the field of clinical disease diagnostics for miR-155.

1. Introduction

Emerging as reliable biomarkers for early cancer diagnosis, microRNAs (miRNAs), a group of noncoding single-strand RNAs, exist in eukaryotic cells and play vital roles in biological processes (Wang et al., 2019). In its regulatory function in gene expression, the abnormal expression of miRNA may be associated with various cancers such as prostate cancer, cervical cancer, and, especially breast cancer (Zeng et al., 2014), afflicting communities worldwide. Furthermore, a recent study has shown that miRNA-155 (miR-155) is frequently over-expressed in breast cancer cases (Mattiske et al., 2012). Tracking the miR-155 concentration would provide references for breast cancer prognosis/diagnosis and for constructing a follow-up survey. Hence, it is imperative to establish an accurate and highly sensitive method for quantitative determination of the miR-155 levels. To date, several analytical methods have been reported for the quantification of miRNAs in multiple samples, of which spectrometry has been frequently used, fluorescent spectrometry (Hong et al., 2016), surface plasmon resonance (Li et al., 2016), surface-enhanced raman spectroscopy (Yang et al., 2018) and ultraviolet spectrophotometry (Hakimian et al., 2018) included. The spectrometric methods exhibit considerable sensitivity to miRNAs but require expensive analytical apparatuses, expertly trained resources and a long runtime for obtaining stable results. Conversely, electrochemical analysis methods that exhibit advantages, including low cost, simple instrumentation, rapid feedback and satisfactory sensitivity, have been used to developed as versatile and powerful biosensors for miRNAs detection. It is worth noting that majority of the electrochemical biosensors fail to perform miRNAs detection without any amplification (e.g. isothermal amplification technologies and nanoprobes) (Hu et al., 2018). Therefore, an appropriate amplification strategy should be integrated with the electrochemical biosensor to detect miRNAs with high sensitivity.

* Corresponding author.
** Corresponding author.
*** Corresponding author.
E-mail addresses: tongh2008@126.com (Y. Tong), luohb77@mail.sysu.edu.cn (H. Luo), chenzg@mail.sysu.edu.cn (Z. Chen).

https://doi.org/10.1016/j.bios.2019.111744
Received 16 July 2019; Received in revised form 16 September 2019; Accepted 28 September 2019
Available online 30 September 2019

Considerable attention should be devoted to nucleic acid-assisted amplification such as rolling circle amplification (Han et al., 2015), hybridization chain reaction (Liu et al., 2015), loop-mediated isothermal amplification (Bartosik et al., 2018) and toehold strand displacement reaction (TSDR) (Li et al., 2019), to improve the electrochemical performance of the biosensor. Clearly, enzyme-assisted amplification considerably enhances the sensitivity and reaction efficiency. However, most of these enzyme-methods require expensive reagents, rigorous conditions, complicated primer design. Furthermore, these methods may yield false positive results (Li et al., 2019). TSDR has been developed as an alternative to detect small molecules (Li et al., 2016) and nucleic acids (Ravan, 2016) by relying on the principle of toehold exchange to output a large numbers of single-strand DNA. In contrast to the remaining enzyme-assisted amplification techniques, TSDR endows the analytical assay with high sensitivity and convenient operation. Here, the rational design of the TSDR system was improved by elongating the DNA shielding region to circumvent the leakage of the DNA trigger (the locked probe) and to minimize the conformational change of the recognition probe by the fuel probe. Such changes can contribute to the development of a facile biosensor for miRNA detection with high sensitivity and low background.

Recently, metal organic frameworks (MOFs) held great potential application in sensing (Hu et al., 2017; Sun et al., 2019). These frameworks possess unique physical and chemical properties such as tunable structures, large surface areas and good stability (Xiong et al., 2015; Liu et al., 2016). The MOF-based sensor is of significant value to develop reliable analytical methods for biomolecule determination (Cui et al., 2015). Further, copper-based MOFs have been commonly used in the electrochemical field because of their interesting peroxidase-like activity, good biocompatibility and biodegradability (Zhou et al., 2018; Rawool and Srivastava, 2019). The unique spherical structure of the copper based MOF synthesized in this study allows it to support nanoparticles of metal and metal oxide catalysts. In addition, endowed with versatile nanozyme-like activity, Pt nanoparticles (PtNPs) are liable to agglomeration due to their high surface e energy, seriously affecting the stability and catalytic ability. Hence, the nanoscale copper-based metal organic framework (Cu-NMOF) may be an ideal candidate for stabilizing PtNPs. Herein, PtNPs were decorated on the surface of Cu-NMOF by *in-situ* reduction to form Cu-NMOF@PtNPs. Horseradish peroxidase (HRP) was attached to the composite material via a metal-protein interaction. The introduction of nanozyme PtNPs and natural HRP was expected to strengthen the catalysis towards hydrogen peroxide (H_2O_2) to achieve signal amplification (Bu et al., 2018). To the best of our knowledge, only few instances of signal amplification based on co-catalytic nanoprobe (Cu-NMOF@PtNPs/HRP) have been reported in the literature. Considering the unique properties of Cu-NMOF@PtNPs/HRP, our group combined the improved cascade strand displacement reaction with a co-catalytic signal probe (Cu-NMOF@PtNPs/HRP, SP) to fabricate a sensitive biosensor for detecting miR-155 with a low detection limit.

Herein, we proposed a facile, highly sensitive biosensor to detect miR-155 using a Cu-NMOF@PtNPs/HRP hybrid nanoprobe and the improved TSDR. Integration of the improved cascade strand displacement amplification with hybrid nanoprobe clearly enhanced the sensitivity of the biosensor. Moreover, the tetrahedral DNA nanostructures (TDNs) were immobilized on the gold electrode (GE) to obtain a stable interface and ensure hybridization efficiency. Because of the combined catalysis of Cu-NMOF, PtNPs and natural HRP, the Cu-NMOF@PtNPs/HRP nanoprobe exhibited outstanding catalytic properties with respect to the hydroquinone-hydrogen peroxide system (HQ-H_2O_2). The facile, fast responding analytical assay showed high sensitivity and stability as well as low detection limits by leveraging the benefits of the synergistically catalytic nanoprobe and the improved TSDR strategy.

2. Experiment section

All experiment procedures are described in supporting information including chemicals, apparatus, cell culture, preparation of nanoprobe and fabrication of biosensor.

3. Results and discussions

3.1. Characterization of Cu-NMOF and Cu-NMOF@PtNPs

The morphologies of Cu-NMOF and Cu-NMOF@PtNPs were characterized by scanning electron microscope (SEM) and transmission electron microscope (TEM). SEM images of Cu-NMOF and Cu-NMOF@PtNPs presented in Fig. 1A and Fig. 1B revealed that Cu-NMOF with a ~200 nm spherical structure was surrounded uniformly by PtNPs after *in-situ* reduction. The TEM results (Fig. 1C and D) further verified that plenty of nanoparticles (~5 nm) covered on the surface of Cu-NMOF, forming a core-satellite nanostructure. Moreover, the morphologies of Cu-NMOF and Cu-NMOF@PtNPs were examined using energy spectrum analysis, elemental mapping analysis, as is shown in Fig. S1 and Fig. S2. It is observed that the peak at 2.08 keV can be assigned to Pt element in the energy spectrum diagram of Cu-NMOF@PtNPs and Cu, C, Pt elements were distributed in Cu-NMOF@PtNPs uniformly. In addition, X-ray photoelectron analysis was performed to characterize Cu-NMOF@PtNPs (Fig. S3). The peak at 314.7 eV and 932.1 eV corresponds to the Pt4d and Cu2p3 lines, assigned to the metallic Pt and Cu. The binding energy (BE) value of Pt4f-Cu3p center at 71 eV and 74 eV, indicating the interaction between Cu-NMOF and PtNPs. All these results above revealed that PtNPs were deposited on the surface of Cu-NMOF successfully.

3.2. The principle of the biosensor

The principle for sensitive detection of miR-155 based on improved cascade amplification and synergistically catalytic nanoprobe is illustrated in Scheme. 1. Cu-NMOF, as a nanocarrier and catalytic material, was synthesized by solvothermal method, with copper nitrate trihydrate and 2-aminoterephthalic acid as precursors and organic ligands. Polyvinylpyrrolidone (PVP) dissolved in a mixed solvent of ethanol and N,N-dimethylformamide was added into the reaction solution to improve the dispersibility of Cu-NMOF in water. After *in-situ* reduction by sodium borohydride ($NaBH_4$), PtNPs were deposited on the surface of the Cu-NMOF. Afterwards, proper concentration of signal DNA and HRP were assembled onto the surface of Cu-NMOF@PtNPs with Pt–S bond and noble metal-protein interaction (Scheme 1A). This prepared signal probe would be applied to amplifying the signal via co-catalyzing electrochemical behavior of the HQ-H_2O_2 system.

The proposed biosensor consisted of TDN supporting substrates, improved TSDR system and co-catalytic nanoprobe (Cu-NMOF@PtNPs/HRP). Firstly, to enhance molecular recognition and the stability of the biosensor, TDNs were immobilized on the interface of GE in order. After blocked by 6-mercapto-1-hexanol (MCH) and bovine serum albumin (BSA) to minimize the non-specificity, the modified electrode was incubated in the mixture (improved TSDR system) containing fuel probe (FP) and the template probe-lock probe-protection probe (TP-LP-PP) complex. In the improved TSDR system, the sequence hybridized with the toehold of the hairpin of TDNs was shielded by the TP. Besides, the TP, LP and PP were primarily denatured together to obtain the stable TP-LP-PP complex to prevent FP from triggering the toehold strand displacement amplification and the conformational change of the hairpin of TDNs in the absence of target (Yang et al., 2018; Zhu et al., 2018). Upon introducing into the system, the target would hybridize with 5′-terminal toehold region (8 nt) of TP to release LP and expose the initially obstructed toehold (4 nt) at the middle position of TP, inducing the second TSDR by fuel strand and the replacement of target, which activated another strand displacement reaction (Scheme 1B).

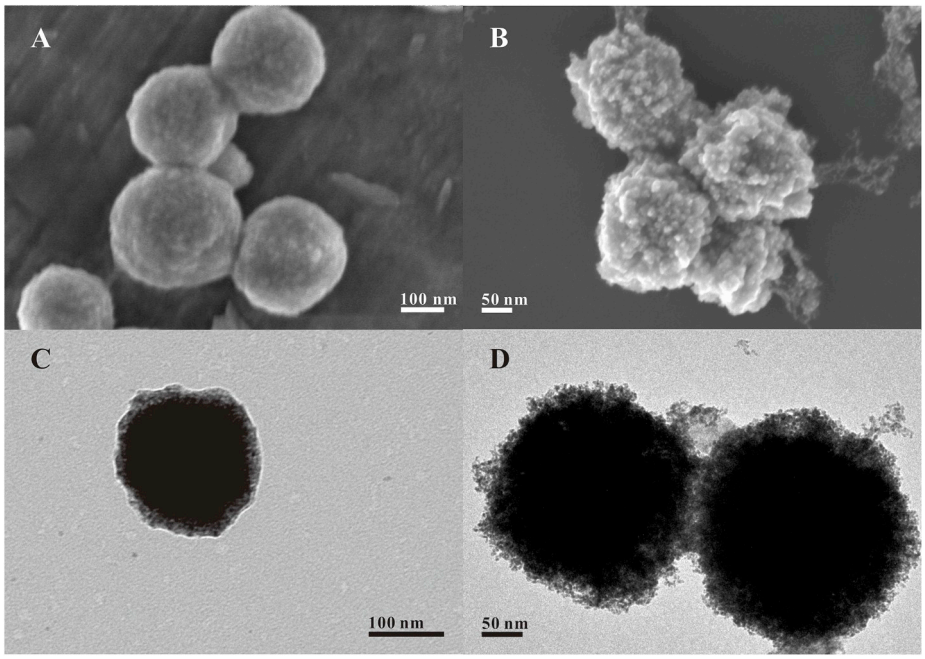

Fig. 1. SEM images of (A) Cu-NMOF and (B) Cu-NMOF@PtNPs, TEM images of (C) Cu-NMOF and (D) Cu-NMOF@PtNPs.

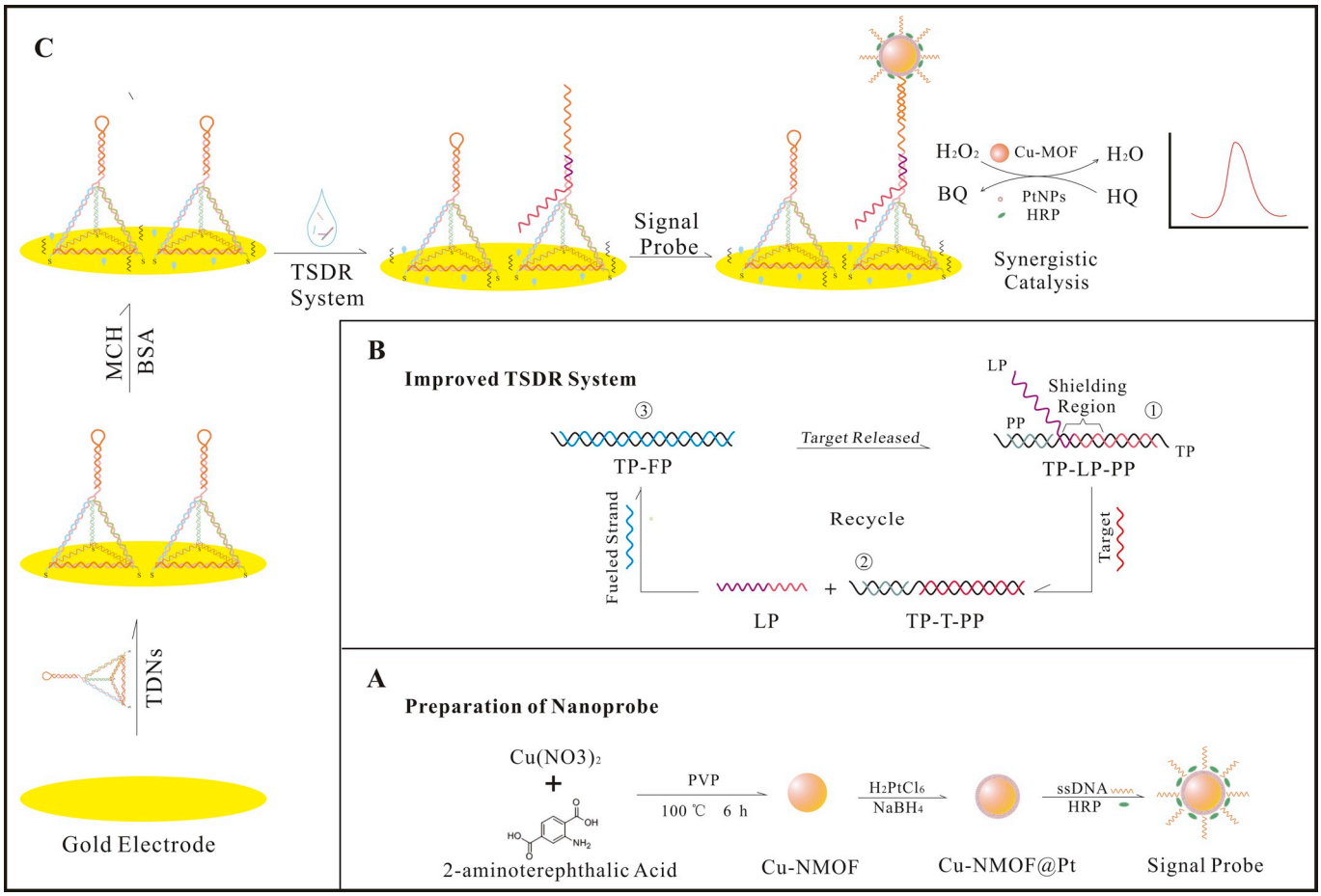

Scheme 1. (A) Preparation process of nanoprobe, (B) Cascade strand displacement system to generate plenty of LP, (C) Schematic illustration of the established platform.

Meanwhile, large numbers of LP released would bind to the hairpin of TDNs immobilized on the electrode and trigger the conformation change of the hairpins. Finally, the signal probe was introduced to form a sandwich structure for amplifying the signal synergistically in the HQ-H_2O_2 based on Cu-NMOF, PtNPs and HRP (Scheme 1C).

3.3. Agarose gel electrophoresis analysis of TDNs and the improved TSDR system

The application of TDNs ensures the orienting ordered arrangement of capture probe on the surface of the electrode to improve the stability of the proposed biosensor. What' more, the independence between TDNs anchored on the electrode and the improved TSDR system is conductive to reducing non-specificity under the coexistence. The formation of TDNs and the improved TSDR system were investigated by agarose gel electrophoresis analysis. As shown in Fig. 2, TDNs in Lane 5 migrated more slowly than other structures assembled by less than four single oligonucleotides (Lane 1–4), demonstrating the successful assembly of TDNs. In the meanwhile, appropriate concentration of TDNs and the improved TSDR system were mixed for 90 min to explore the feasibility of the proposed strategy. Compared with positive reaction (Lane 8), the band of TDN-LP complex could not be observed, revealing that TDNs can coexist with the improved TSDR system without miR-155 (Lane 7). Instead, the DNA machine would generate large numbers of LP to hybridize with TDNs. The separated DNA (Lane 9) was in line with positive reaction, manifesting the practicability of this strategy.

3.4. Electrochemical characterization of the constructed biosensor

In order to characterize the stepwise assembly process on the surface of the established platform, electrochemical impedance spectroscopy (EIS) was adopted in PBS containing 5 mM $Fe(CN)_6^{3-/4-}$ and 0.5 M KCl. In the Nyquist plot, the semicircle diameter in the high frequency region mirrored the electron-transfer resistance (R_{et}). As seen in Fig. 3A, when the TDNs were self-assembled on the electrode via Au–S bond, the R_{et} increased to 750 Ω owing to the repulsion between negatively charged phosphate backbones of DNA (curve a). After blocking by MCH and BSA,

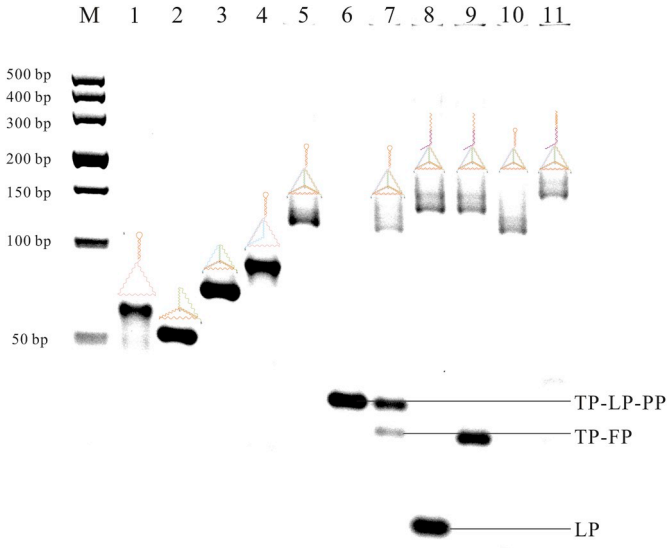

Fig. 2. Agarose gel electrophoretic analysis of the formation of TDNs and TSDR system. Lane 1: A; Lane 2: B + C; Lane 3: B + C + D; Lane 4: A + D; Lane 5: A + B + C + D; Lane 6: TP-LP-PP; Lane 7: TDNs + TP-LP-PP + FP; Lane 8: TDNs + LP; Lane 9: TDNs + TP-LP-PP + FP + miR-155; Lane 10: TDNs + signal probe; Lane 11: TDNs + LP + signal probe. With the exception for LP in positive control (2.0 μM), target (0.02 μM), DNA final concentration of L1-L6 and L7-L11 were 1.0 μM and 0.5 μM respectively.

the R_{et} further increased to 1300 Ω and 1850 Ω respectively (curve b, c). Subsequently, with TSDR system incubation, obvious increase could be observed (curve d) because large numbers of LP hybridized with TDNs on the surface and the formation of the DNA complex with more strongly negative change further impeded electron transfer. Finally, the prepared signal probe bind with the released stem of TDNs, which resulted in the diameter of semicircle further increased to 3750 Ω (curve e), evidencing that the proposed platform for miR-155 was successfully constructed.

Additionally, Fig. 3B showed that SWVs of different process in the PBS solution (100 mM, pH 7.0) with 3 mM HQ and 2 mM H_2O_2 bubbled with nitrogen. A weak cathodic peak, corresponding to the electrochemical reduction of benzoquinone (BQ) which was generated from the oxidation of HQ by catalyzing H_2O_2, could be observed in the absence of target (curve a). When the FPs were removed from the amplification strategy and the platform was performed with pristine Cu-NMOF@PtNPs/HRP, the peak current of the biosensor was 5.8 μA (curve b), revealing the considerable catalytic-property of the nanoprobe. Moreover, the currents based on the improved TSDR and co-catalytic signal probe doubled those without the FPs at the same concentrations of target (curve c), because the FPs were essential for cascade amplification by liberating the target hybridized with TP, which would activate another strand displacement reaction. Therefore, the established biosensor may be a proper electrochemical platform for detection of miR-155.

Furthermore, PtNPs/HRP widely used in electrochemical biosensor as signal probe, was synthesized by previous report (Sun et al., 2018) and served as a comparison to evaluate the catalytic activity of Cu-NMOF@PtNPs and Cu-NMOF@PtNPs/HRP. The catalytic property of different signal probes including PtNPs/HRP, Cu-NMOF@PtNPs/HRP and enzyme-free Cu-NMOF@PtNPs was investigated by SWVs using different signal probe in the PBS solution (100 mM, pH 7.0) with 3 mM HQ and 2 mM H_2O_2 (Fig. 3C). After incubation of the improved TSDR and PtNPs/HRP, a weak cathodic peak appeared in the potential range of 0.1～-0.6 V. Nevertheless, the reduction peak increased dramatically when Cu-NMOF@PtNPs and Cu-NMOF@PtNPs/HRP was employed on the biosensor. The peak current with PtNPs/HRP, Cu-NMOF@PtNPs and Cu-NMOF@PtNPs/HRP towards miR-155 were 1.3 μA, 3.7 μA and 6.4 μA, respectively. Probably the enhance signal were attributed to the synergistically catalytic effect of Cu-NMOF, PtNPs and natural HRP. Cu-NMOF with mimicking peroxidase activity provided more spatial position to immobilize PtNPs, which further strengthen the catalytic effect towards H_2O_2. Moreover, the attachment of HRP on the surface of Cu-NMOF@PtNPs via metal-protein interaction, resulting in catalysis of H_2O_2 with higher efficiency. Besides, UV–vis spectra of different signal probe (Fig. S4) were introduced as an assisted characterization to investigate the catalytic ability of H_2O_2. As suggested in Fig. S4, Cu-NMOF@PtNPs/HRP possessed the more prominent catalytic effect towards H_2O_2, which are in accord with the results of SWVs.

3.5. Optimization of the experiment conditions

The combination of the improved toehold mediated strand displacement reaction and co-catalysis nanoprobe tremendously improve the sensitivity of the biosensor. However, because of the cascade amplification of TSDR, the leakage of LP without target would be amplified by synergistically catalytic nanoprobe, resulting in the higher background current. Therefore, it is of important significance for inhibition of nonspecific reaction in TSDR. To obtain the optimal conditions to ameliorate electrochemical performance, the number of shielding base in TSDR was investigated by SWV in PBS solution containing 3 mM HQ and 2 mM H_2O_2. As can be seen in Fig. 4A, with increasing the number of shielding base, the cathodic current increased notably in 1 pM target (blue line) while the current decreased without target (red line) for the reason of the enhancement of independence between the TP-LP-PP complex and the hairpin of TDNs. The sequence of hybridization region between TP and LP overlapped with the stem of the

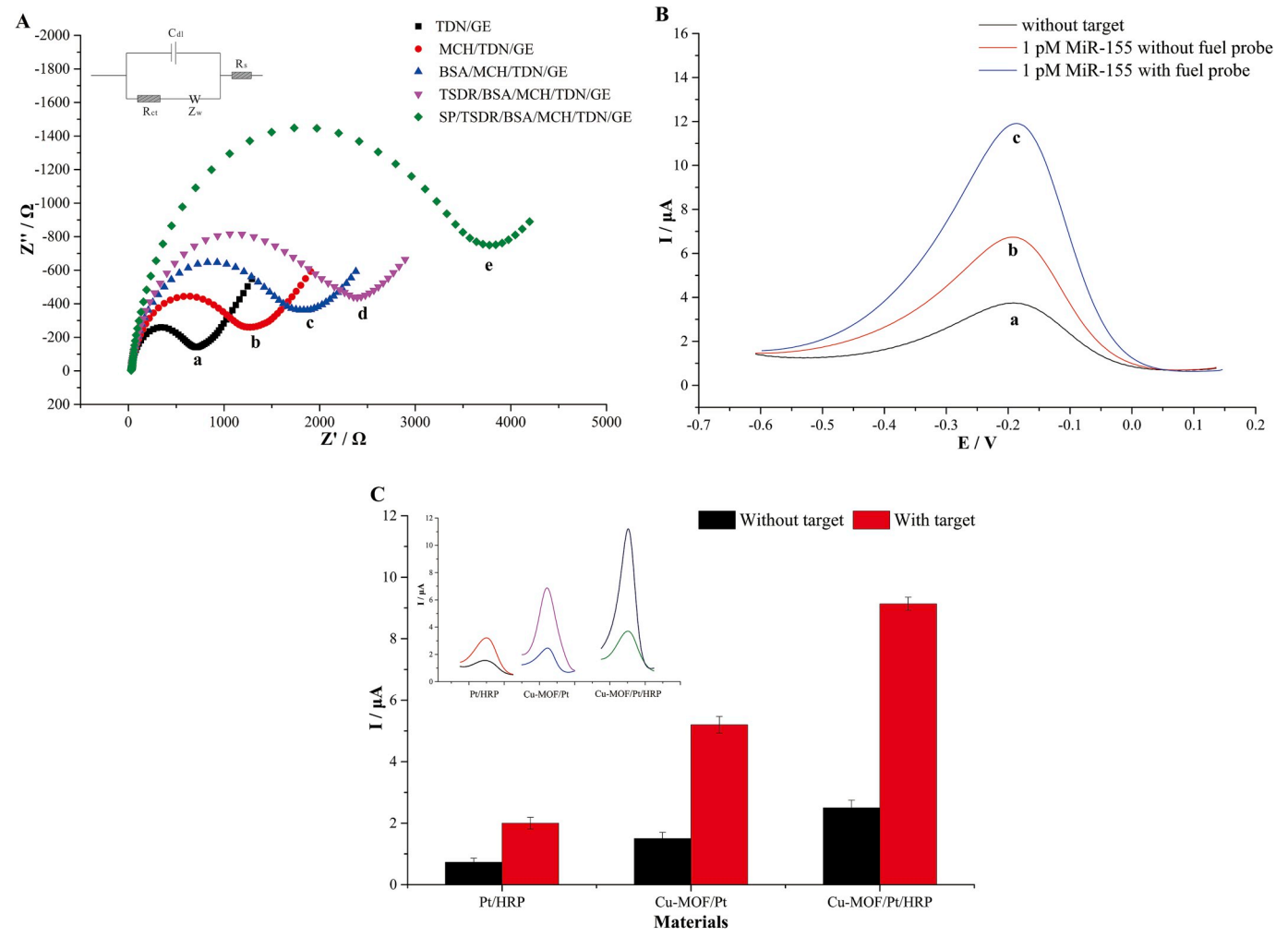

Fig. 3. (A) Nyquist plots of the developed biosensor. (a) TDN/GE, (b) MCH/TDN/GE, (c) BSA/MCH/TDN/GE, (d) TSDR/BSA/MCH/TDN/GE, (e) SP/TSDR/BSA/MCH/TDN/GE. (B) SWV responses of the (a) SP/TSDR/MCH/TDN/GE without target, (b) SP/MCH/TDN/GE with 1 pM target, (c) SP/TSDR/MCH/TDN/GE with 1 pM target in the PBS solution (100 mM, pH 7.0) with 3 mM HQ and 2 mM H_2O_2. (C) SWV responses of different probe with 1 pM target in the PBS solution (100 mM, pH 7.0) with 3 mM HQ and 2 mM H_2O_2. Inset of a: SWVS of cathodic currents versus different signal probes.

hairpin of TDNs and the leakage of LP would greatly improve. When the shielding number of base was over 14 mers, the target may bind with the hairpin of TDNs directly instead of involving in TSDR, resulting in the rise in cathodic current. Likewise, the current with fuel strand surged dramatically (black line) because a large concentration of fuel probes with partially repetitive sequence may open the hairpin immobilized on the biosensor falsely, which coincided with the reported (Gao et al., 2016). Taking account of all of these, 14 shielding base was selected as the optimal condition for this improved TSDR system.

Similarly, the incubation time of the improved TSDR significantly affected the cathodic current by influencing the output of LP (Shi et al., 2015). Hence, an optimization procedure on the incubation time of TSDR was executed (Fig. 4B). The influence of TSDR incubation time at the concentration of 1 pM target was evaluated by recording SWVs. As anticipated, the peak currents become higher with the increase in incubation time and the current reach the maximum when the incubation time was 90 min. The current tends to be stable when the time exceeds 90 min, indicating that the release of LP may achieve equilibrium of cascade displacement amplification. As a consequence, the improve toehold strand amplification was incubated on the GE for 90 min in the subsequent experiments.

Finally, the hybridization time of the nanoprobe was investigated thoroughly by SWVs (Fig. 4C). Fig. 4C present the SWV responses of different hybridization time (40, 50, 60, 70, 80 and 90 min) of signal probe after 90 min improved TSDR incubation. The peak current at this biosensor was enhanced by signal probe with a rise in hybridization time and reached to the stability after 70 min. An appropriate hybridization time of the nanoprobe would help prevent physical adsorption of nanomaterial. Thus, the optimal signal-probe incubation time was 70 min in this platform.

3.6. *Analytical performance of the miRNA detection*

Under optimal experiment conditions, the electrochemical analysis of miR-155 with different concentrations were evaluated by SWVs and recorded in Fig. 5A. Fig. 5A revealed variations of miR-155 concentration ranging from 0.5 to 10^5 pM and the cathodic currents of miR-155 at the potentials of 0.1~-0.6 V. Change of the logarithm of miR-155 concentration, led to the linear variation of cathodic current (Fig. 5B). The regression equation was I (μA) = 1.730 Lg c (mol·L^{-1}) +30.93 with a regression coefficient (R) of 0.9974. The detection limit for miR-155 was calculated to be 0.13 fM with 3σ. Compared with other strategies towards microRNA summarized in Table S2, the biosensor in this work offers a wider linear range and a lower detection limit, which is superior to some reported methods. The performances of the biosensor are attributed to the following points. Firstly, TDNs immobilized on the GE in order enhances the stability of the biosensor and the binding efficiency of the improved TSDR products. Besides, the rational designed of

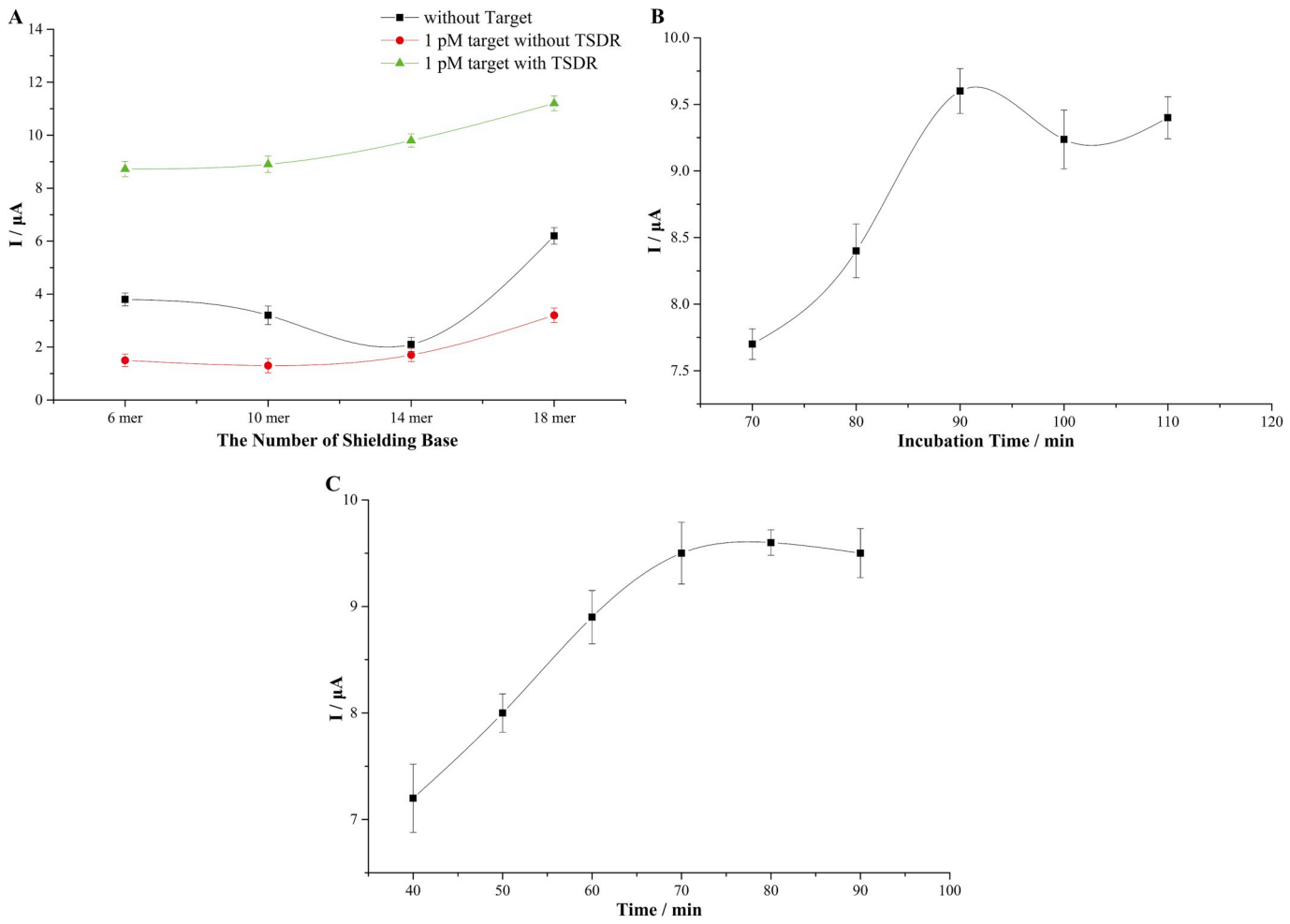

Fig. 4. (A) Effects of shielding number of TSDR system on SWV response. (B) Effects of TSDR incubation time on SWV response at 1 pM miR-155. (C) Effects of signal probe hybridization time on SWV response at 1 pM miR-155.

the improved TSDR system minimize non-specific reaction and proved a lower background currents. The last but not the least, because of the combined catalysis of Cu-NMOF, PtNPs and natural HRP, the hybrid nanoprobe exhibits extraordinary catalysis with respect to the HQ-H_2O_2 system, which will contribute to the multiple amplification. All of the above factors endows the proposed biosensor with high sensitivity and stability.

3.7. Stability, reproducibility and selectivity of the constructed biosensor

To validate the stability of the electrode fabricated, the biosensors modified by TDNs were immersed in PBS and stored at 4 °C for half a month, the cathodic currents of 1 pM miR-155 were still as high as 92.4% and the relative standard deviations (RSDs) were 4.7%. Thus, the proposed platform was highly stable. Additionally, five different electrodes assembled independently contrived to determine 1 pM miR-155 with RSD of 3.1%, demonstrating the established electrode has a satisfactory reproducibility.

Moreover, the effect of a variety of miRNAs coexisted in real sample obsess us to detect miR-155, leading to false-positive result. Hence, the electrochemical performances of interfering substances such as miR-21, single-base mismatch miR-155 (SM miR-155), three-base mismatch miR-155 (TM miR-155) and their mixture, were performed to investigate the selectivity of the constructed biosensor (Fig. 5C). It turns out that, 100 fold miR-21, SM miR-155, TM miR-155 as well as the mixture containing 100 fold SM miR-155, TM miR-155, 1 fold miR-21 failed to influence the detection of 1 pM miR-155, confirming the high selectivity of the proposed biosensor used for miR-155 determination.

3.8. Real sample analysis

To prove the practicability of the established biosensor for detection of miR-155, the platform was applied to the determination of miR-155 in serum (Table S3) and cell lysates (Fig. S5). Each sample of miR-155 was determined in triplicate. Various concentration of miR-155 spiked into the human blood serum (100-fold diluted) were involved in TSDR system and activated the DNA molecular machine. The recoveries of miR-155 in serum ranged from 93.1% to 109.0% and the RSD were lower than 5.0%, indicating that the platform is competent for the detection of miR-155 in serum.

Moreover, we examined the expression of miR-155 in the different biological lysates (Fig. S5). MCF-7 and MDA-MB-231 were extracted by SanPrep Column microRNA Extraction Kit after cell counting. As expected, the current signal were relevant to the number of cancer cells used for miR-155 extraction. With the number of cells in rise, the reduction current increased in different degrees, which are consistent with previous literatures (Mohammadi and Salim, 2018; Zhang et al., 2018; Zhou et al., 2016; Lu et al., 2009). Therefore, the novel sensors constructed was reliable and applicable to detection of miR-155 in biological samples.

4. Conclusion

Based on improved cascade strand displacement amplification and

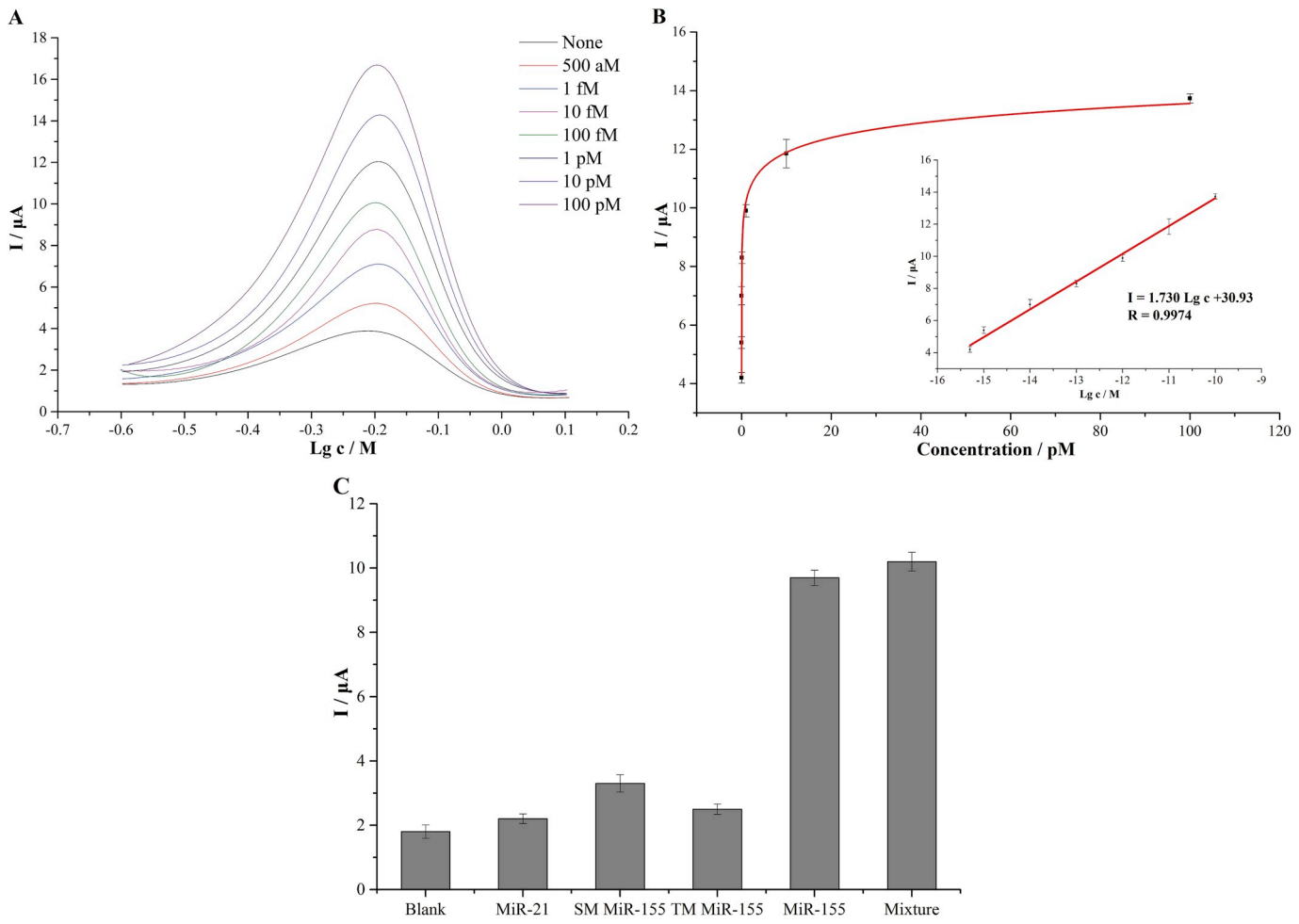

Fig. 5. (A) SWV curves responding to different miRNA concentrations. (B) Linear relationship between the current variation, and the logarithm of the miRNA concentration. (C) Selectivity of the sensor hybridized to different miRNA sequences (the concentration of miRNA 155 is 1 pM, each interference is 100 pM, the mixture contains 1 pM of miRNA 21, miR-155 with 100 pM of SM miR-155 and TM miR-155).

synergistically catalytic nanoprobe, a novel and facile electrochemical biosensor was fabricated to detect miR-155, with a low detection limit. Compared with pristine PtNPs/HRP and Cu-NMOF@PtNPs, the nanoprobe showed superb co-catalytic property with respect to the HQ-H_2O_2 system, which indirectly amplify the cathodic signal of BQ. Under optimal conditions, the cathodic current was logarithmically related with 0.50–1.0 $\times 10^5$ fM miR-155 with a detection limit of 0.13 fM. Above all, owing to the extraordinary catalytic activity along with high sensitivity and stability, the established platform was available for determination of miR-155 in serum and biological samples, opening up possibilities for early diagnosis and treatment of breast cancer in the future. Despite significant development in miR-155 detection, the established platform may not be an ideal method for clinical detection yet. With the miRNA detection consummating further, future electrochemical biosensor of miRNA detection would march towards rapidness, integration and microminiaturization.

Declaration of competing interest

The authors declare that they have no known competing financial interests or personal relationships that could have appeared to influence the work reported in this paper.

CRediT authorship contribution statement

Zhixian Liang: Conceptualization, Investigation, Methodology, Supervision, Validation, Writing - original draft, Writing - review & editing. **Dan Ou:** Writing - original draft, Writing - review & editing. **Duanping Sun:** Funding acquisition, Resources, Software, Writing - review & editing. **Yanli Tong:** Formal analysis, Resources. **Haibin Luo:** Visualization. **Zuanguang Chen:** Funding acquisition, Project administration.

Acknowledge

We gratefully acknowledge the National Natural Science Foundation of China (No. 21675177), the Natural Science Foundation of Guangdong Province (No. 2018A030310142), the Science and Technology Planning Project of Guangdong Province (No. 2016B030303002), the Medical Scientific Research Foundation of Guangdong Province (No. A2017033) and the Fundamental Research Funds for the Central Universities (NO. 18ZXXT69).

Appendix A. Supplementary data

Supplementary data to this article can be found online at https://doi.org/10.1016/j.bios.2019.111744.

References

Bartosik, M., Jirakova, L., Anton, M., Vojtesek, B., Hrstka, R., 2018. Anal. Chim. Acta 1042, 37–43.
Bu, X.N., Fu, Y.X., Jin, H., Gui, R.J., 2018. New J. Chem. 42, 17323–17330.

Cui, L., Wu, J., Li, J., Ju, H.X., 2015. Anal. Chem. 87, 10635–10641.
Gao, Y.F., Xu, J., Li, B.X., Jin, Y., 2016. Biosens. Bioelectron. 81, 415–422.
Hakimian, F., Ghourchian, H., Hashemi, A.S., Arastoo, M.R., Rad, M.B., 2018. Sci. Rep. 8, 2943.
Han, D., Wu, C.C., You, M.X., Zhang, T., Wan, S., Chen, T., Qiu, L.P., Zheng, Z., Liang, H., Tan, W.H., 2015. Nat. Chem. 7, 835–841.
Hong, C., Baek, A., Hah, S.S., Jung, W., Kim, D.E., 2016. Anal. Chem. 88, 2999–3003.
Hu, F., Zhang, W.C., Zhang, J.Q., Zhang, Q., Sheng, T., Gu, Y.Q., 2018. Sens. Actuators B Chem. 271, 15–23.
Hu, S.S., Ouyang, W.J., Guo, L.H., Lin, Z.Y., Jiang, X.H., Qiu, B., Chen, G.N., 2017. Biosens. Bioelectron. 92, 718–723.
Li, Q., Liu, Z., Zhou, D.H., Pan, J.F., Liu, C.S., Chen, J.H., 2019. Analyst 144, 2173–2178.
Li, X., Peng, Y., Chai, Y.Q., Yuan, R., Xiang, Y., 2016. Chem. Commun. 52, 3673–3676.
Li, X.M., Cheng, W., Li, D.D., Wu, J.L., Ding, X.J., Cheng, Q., Ding, S.J., 2016. Biosens. Bioelectron. 80, 98–104.
Li, Y.J., Ding, X.J., Li, D.D., Wu, H.P., Huang, W., Ding, S.J., 2019. Anal. Methods 11, 1613–1619.
Liu, L.L., Song, Y.B., Chong, H.B., Yang, S., Xiang, J., Jin, S., Kang, X., Zhang, J., Yu, H.Z., Zhu, M.Z., 2016. Nanoscale 8, 1407–1412.
Liu, L.Z., Song, C., Zhang, Z., Yang, J., Zhou, L.L., Zhang, X., Xie, G.M., 2015. Biosens. Bioelectron. 70, 351–357.
Lu, Y.J., Xiao, J.N., Lin, H.X., Bai, Y.L., Luo, X.B., Wang, Z.G., Yang, B.F., 2009. Nucleic Acids Res. 37, e24.
Mattiske, S., Suetani, R.J., Neilsen, P.M., Callen, D.F., 2012. Cancer Epidemiol. Biomark. Prev. 21, 1236–1243.
Mohammadi, S., Salim, A., 2018. Microchim. Acta. 185, 372.
Ravan, H., 2016. Anal. Chim. Acta 910, 68–74.
Rawool, C.R., Srivastava, A.K., 2019. Sens. Actuators B Chem. 288, 493–506.
Shi, K., Dou, B.T., Yang, C.Y., Chai, Y.Q., Yuan, R., Xiang, Y., 2015. Anal. Chem. 87, 8578–8583.
Sun, D.P., Lu, J., Luo, Z.F., Zhang, L.Y., Liu, P.Q., Chen, Z.G., 2018. Biosens. Bioelectron. 120, 8–14.
Sun, Y.J., Jiang, X.W., Jin, H., Gui, R.J., 2019. Anal. Chim. Acta. https://doi.org/10.1016/j.aca.2019.07.027.
Wang, S., Wang, L., Xu, X.W., Li, X., Jiang, W., 2019. Anal. Chim. Acta 1063, 152–158.
Xiong, C.Y., Wang, H.J., Liang, W.B., Yuan, Y.L., Yuan, R., Chai, Y.Q., 2015. Chem. Eur J. 21, 9825–9832.
Yang, J.M., Wu, Y.L., Gan, C.F., Yuan, R., Xiang, Y., 2018. Biosens. Bioelectron. 117, 743–747.
Yang, X., Wang, S.F., Wang, Y., He, Y., Chai, Y.Q., Yuan, R., 2018. ACS Appl. Mater. Interfaces 10, 12491–12496.
Zeng, H., Fang, C., Nam, S.Y., Cai, Q., Long, X.H., 2014. BioMed Res. Int. 2014, 724209.
Zhang, Y., Li, X., Xu, Z.Q., Chai, Y.Q., Wang, H.J., Yuan, R., 2018. Chem. Commun. 54, 10148–10151.
Zhou, W.J., Li, D.X., Xiong, C.Y., Yuan, R., Xiang, Y., 2016. ACS Appl. Mater. Interfaces 8, 13303–13308.
Zhou, Y.L., Li, C.M., Hao, Y.Q., Ye, B.X., Xu, M.T., 2018. Talanta 188, 282–287.
Zhu, J., Gan, H.Y., Wu, J., Ju, H.X., 2018. Anal. Chem. 90, 5503–5508.